Synthesis, Structure, and the Unusual Magnetic Properties of an Amine-Templated Iron(II) Sulfate Possessing the Kagomé Lattice

C. N. R. Rao,*[,†,‡] E. V. Sampathkumaran,[§] R. Nagarajan,[§] Geo Paul,[†] J. N. Behera,[†,‡] and Amitava Choudhury[†,‡]

Chemistry and Physics of Materials Unit and CSIR Center of Excellence in Chemistry, Jawaharlal Nehru Centre for Advanced Scientific Research, Jakkur P.O., Bangalore 560 064, India, Solid State and Structural Chemistry Unit, Indian Institute of Science, Bangalore 560 012, India, and Department of Condensed Matter Physics and Materials Science, Tata Institute of Fundamental Research, Mumbai 400 005, India

Received December 10, 2003. Revised Manuscript Received January 31, 2004

An amine-templated iron(II) sulfate of the composition $[H_3N(CH_2)_6NH_3]$ $[Fe^{II}_{1.5}F_3(SO_4)]\cdot 0.5H_2O$, **I**, representing an example of a Kagomé lattice with Fe in the +2 state, has been synthesized under solvothermal conditions. Having determined the structure by single-crystal X-ray diffraction, the oxidation state of iron was established by Mössbauer spectroscopy. The magnetic properties of the Fe(II) Kagomé compound are rather unusual in that it undergoes ferrimagnetic ordering below 19 K and does not exhibit spin-glass freezing.

Introduction

Although there is extensive literature on the open-framework structures of metal silicates,[1] phosphates,[2] and so on, it is only recently that open-framework structures involving anions such as selenite[3] and sulfate[4] have also been discovered. Thus, the synthesis and characterization of several organically templated layered and three-dimensional metal sulfates have been reported recently.[4] In particular, the structure and properties of several layered iron sulfates have been examined as part of such studies.[4c,4d,5] To our knowledge, all the iron compounds with the Kagomé lattice reported hitherto in the literature generally possess Fe in the +3 state (d^5).[6] These Kagomé compounds exhibit magnetic frustration or long-range antiferromagnetism at low temperatures. In this paper, we report the synthesis and structure of an amine-templated iron(II) sulfate possessing a perfect Kagomé lattice, with the composition $[H_3N(CH_2)_6NH_3][Fe^{II}_{1.5}F_3(SO_4)]\cdot 0.5H_2O$, **I**. **I** contains Fe^{2+} (d^6) and exhibits unusual magnetic properties, distinctly different from those of the Fe^{3+} Kagomé lattices reported in the literature.[6] Accordingly, we observe a ferrimagnetic transition besides a possible structural transition in an unusual example of Fe(II) Kagomé compound.

Experimental Section

Synthesis and Initial Characterization. Compound **I** was synthesized under mild hydro-/solvothermal conditions. In a typical synthesis, 0.2630 g of iron(III) citrate was dispersed in 5.6/1.8 mL of *n*-butanol/H_2O under constant stirring. To this mixture was added 0.4648 g of 1,6-hexamethylenediamine (HMDA) and 0.16 mL of sulfuric acid (98%) followed by the addition of 0.18 mL of HF (40%) and the mixture was stirred for 30 min. The final mixture with the molar composition of 1:3:4:60:100:4 iron(III) citrate:H_2SO_4:HMDA:*n*-butanol:H_2O:HF with an initial pH of 4 was transferred into a 23-mL PTFE-lined acid digestion bomb and heated at 150 °C for 2 days. The product, containing pale yellow hexagonal plate-shaped crystals (yield 80%, with respect to Fe) was filtered and washed with water. No appreciable change in the pH was observed in the supernatant after the reaction. The compound **I** was characterized by single-crystal X-ray diffraction, powder X-ray diffraction (XRD), thermogravimetric analysis (TGA), energy-dispersive X-ray analysis (EDAX), elemental CHN analysis, IR spectroscopy, and Mössbauer spectroscopy. Magnetic measurements on powdered samples were performed at temperatures between 2 and 300 K, using a Quantum Design SQUID magnetometer. The Mössbauer spectra were taken in a home-built constant acceleration Mössbauer spectrometer

* To whom correspondence should be addressed. E-mail: cnrrao@jncasr.ac.in.

† Jawaharlal Nehru Centre for Advanced Scientific Research.

‡ Indian Institute of Science.

§ Tata Institute of Fundamental Research.

(1) (a) Breck, D. W. *Zeolite Molecular Sieves; Structure, chemistry and use*; J. Wiley and Sons: New York, 1974. (b) Baerlocher, C.; Meier, W. M.; Olson, D. H. *Atlas of Zeolite Framework Types*, 5th ed.; Elsevier: Amsterdam, 2001.

(2) (a) Cheetham, A. K.; Férey, G.; Loiseau, T. *Angew. Chem., Int. Ed.* **1999**, *38*, 3268. (b) Rao, C. N. R.; Natarajan, S.; Choudhury, A.; Neeraj, S.; Ayi, A. A. *Acc. Chem. Res.* **2001**, *34*, 80.

(3) (a) Choudhury, A.; Udayakumar D.; Rao, C. N. R. *Angew. Chem., Int. Ed.* **2002**, *41*, 158. (b) Harrison, W. T. A.; Phillips, M. L. F.; Stanchfield, J.; Nenoff, T. M. *Angew. Chem., Int. Ed.* **2000**, *39*, 3808.

(4) (a) Choudhury, A.; Krishnamoorthy, J.; Rao, C. N. R. *Chem. Commun.* **2001**, 2610. (b) Paul, G.; Choudhury, A.; Rao, C. N. R. *J. Chem. Soc., Dalton Trans.* **2002**, 3859. (c) Paul, G.; Choudhury, A.; Rao, C. N. R. *Chem. Commun.* **2002**, 1904. (d) Paul, G.; Choudhury, A.; Rao, C. N. R. *Chem. Mater.* **2003**, *15*, 1174. (e) Doran, M.; Norquist, A. J.; O'Hare, D. *Chem. Commun.* **2002**, 2946.

(5) (a) Paul, G.; Choudhury, A.; Sampathkumaran, E. V.; Rao, C. N. R. *Angew. Chem., Int. Ed.* **2002**, *41*, 4297. (b) Rao, C. N. R.; Paul, G.; Choudhury, A.; Sampathkumaran, E. V.; Raychaudhuri, A. K.; Ramasesha, S.; Rudra, I. *Phys. Rev. B* **2003**, *67*, 134425.

(6) (a) Ramirez, A. P. *Annu. Rev. Mater. Sci.* **1994**, *24*, 453. (b) Greedan, J. E. *J. Mater. Chem.* **2001**, *11*, 37. (c) Wills, A. S.; Harrison, A. *J. Chem. Soc., Faraday Trans.* **1996**, *92*, 2161. (d) Inami, T.; Nishiyama, M.; Maegawa, S.; Oka, Y. *Phys. Rev. B* **2000**, *61*, 12 181. (e) Reimers, J. N.; Berlinsky, A. J. *Phys. Rev. B* **1993**, *48*, 9539. (f) Frunzke, J.; Hansen, T.; Harrison, A.; Lord, J. S.; Oakley, G. S.; Visser, D.; Wills, A. S. *J. Mater. Chem.* **2001**, *11*, 179.

10.1021/cm035304+ CCC: $27.50
Published on Web 03/11/2004

with a ^{57}Co source in Rh matrix. Sample temperature was varied in a flow-type cryostat. The velocity calibration was performed with an α-Fe foil at room temperature and the measured chemical shifts are with respect to this α-Fe standard.

The C, H, N analysis [(in wt %) C, 19.55; N, 7.57; H, 5.30 (calc.: C, 19.77; N, 7.69; H, 5.21)] was in good agreement with the formula $[H_3N(CH_2)_6NH_3][Fe^{II}_{1.5}F_3(SO_4)]\cdot 0.5H_2O$, **I**, derived from crystallography. EDX analysis indicated the ratio of Fe and S to be 3:2 in **I** in accordance with the formula. The water content of **I** was established independently by TGA to be close to the expected value. The TGA curve (N_2 atmosphere, range 30−900 °C, heating rate 5 °C/min) of **I** showed distinct weight losses consistent with the molecular formula. TGA of **I** reveals the loss of guest water molecules at 150 °C [obs = 2.5%, calc = 2.47%] and a sharp weight loss around 300 °C corresponding to the loss of the amine and HF [HMDA + 2HF, obs = 42.84%, calc = 42.80%]. The second major weight loss in the region 400−500 °C corresponds to the removal of remaining fluorine and the decomposition of SO_4^{2-} moiety, [$0.5F_2 + SO_2 + 0.5O_2$, obs = 25.10%, calc = 22.47%]. The sample heated at 850 °C diffracts weakly and the PXRD corresponds to Fe_2O_3 (JCPDS file, card no. = 33-0664). The presence of fluorine atoms was also confirmed by the qualitative analysis of **I** and their locations being supported by the bond valence sum calculations as well. The %F values found from the quantitative estimates of all the other elements in **I** match the proposed formula.

IR spectrum of **I** exhibits characteristic bands of the amine and water molecules. The broad bands due to ν(O−H) and ν(N−H) are observed in the 3200−3500-cm^{-1} region while the bending modes for the amine and water are observed in the range 1300−1650 cm^{-1}. The spectrum of **I** shows multiple strong bands in the 900−1040-cm^{-1} region due to ν_1 and in the 1050−1250-cm^{-1} region due to ν_3 vibration modes of the sulfate group.[7] The bending modes of SO_4^{2-} are found in the 400−500- and 600−795-cm^{-1} regions.

Single-Crystal Structure Determination. Suitable single crystal of **I** was carefully selected under a polarizing microscope and glued to a thin glass fiber with cyanoacrylate (superglue) adhesive. Single-crystal data were collected on a Siemens SMART-CCD diffractometer [graphite-monochromated Mo Kα radiation, λ = 0.71073 Å (T = 298 K)]. An absorption correction based on symmetry-equivalent reflections was applied using SADABS.[8] The structure was solved by direct method using SHELXS-86[9] and difference Fourier synthesis. The direct method solution readily revealed the heavy atom positions (Fe and S) and facilitated the identification of most of the other fragments (O, F, C, N, and H) from difference Fourier maps. Hydrogen positions were initially located in the difference Fourier maps, and for the final refinement, the hydrogen atoms were placed geometrically and held in the riding mode. Hydrogen atoms for the disordered guest water molecule were not added for the final refinements. The last cycles of refinement included atomic positions for all the atoms, anisotropic thermal parameters for the nonhydrogen atoms, and isotropic thermal parameters for all the hydrogen atoms. Full-matrix least-squares structure refinement against $|F^2|$ was carried out using SHELXTL-PLUS[10] package of programs. Details of the final refinements are given in Table 1. The positions of the fluorine atoms are located primarily by looking at their thermal parameters; assigning them as oxygen atoms instead of fluorine invariably leads to nonpositive definite values when they were refined with anisotropic displacement parameters. The powder X-ray diffraction pattern of the compound was in good agreement with the simulated patterns generated from the single-crystal XRD data, indicating the phase purity of the compound. Selected values of the bond distances and bond angles for **I** are listed in Table 2. Various hydrogen bond interactions in **I** are listed in Table 3.

Table 1. Crystal Data and Structure Refinement Parameters for I

empirical formula	$[H_3N(CH_2)_6NH_3][Fe^{II}_{1.5}F_3(SO_4)]\cdot 0.5H_2O$
formula weight	364.08
space group	*C*2/*m*
a, Å	12.830(7)
b, Å	7.334(8)
c, Å	13.319(9)
α, deg	90
β, deg	98.724(2)
γ, deg	90
V, Å^3	1239.0(2)
Z	8
T °C	20
λ (Mo Kα), Å	0.71073
θ range, deg	1.55−23.26
ρ_{calc}, g cm^{-3}	1.907
μ, mm^{-1}	1.498
R1[a]	0.0336
wR2[b]	0.0856

[a] $R1=\sum||F_o| - |F_c||/\sum|F_o|$. [b] $wR2 = \{\sum[w(F_o^2 - F_c^2)^2]/\sum[w(F_o^2)^2]\}^{1/2}$, $w = 1/[\sigma^2(F_o)^2 + (aP)^2 + bP]$, $P = [F_o^2 + 2F_c^2]/3$, where $a = 0.0596$ and $b = 0.000$ for **I**.

Results and Discussion

The asymmetric unit (Figure 1a) of $[H_3N(CH_2)_6NH_3][Fe^{II}_{1.5}F_3(SO_4)]\cdot 0.5H_2O$, **I**, contains 17 non-hydrogen atoms, out of which 8 belong to the inorganic framework and 9 belong to the extraframework guest molecules, including a water molecule. The structure of **I** consists of anionic layers of vertex-sharing $Fe^{II}F_4O_2$ octahedra and tetrahedral SO_4 units, which are fused together by Fe−F−Fe and Fe−O−S bonds. Each FeF_4O_2 unit shares four of its Fe−F vertexes with similar neighbors, with the Fe−F−Fe bonds nearly aligned in the *ab*-plane. The Fe−O bond is canted from the *ab*-plane and the Fe−O vertex effectively forces a three-ring trio of apical Fe−O bonds closer together to allow them to be capped by the SO_4 tetrahedra. The three- and six-rings of the octahedra resulting from the in-plane connectivity is shown in Figure 1b. The layers in **I** are typical of a Kagomé lattice, with hexagonal tungsten bronze-type sheets of vertex-sharing FeF_4O_2 octahedra as shown in Figure 1b. This structure is akin to that of the mineral jarosite[11] where all the Fe atoms are in the +3 oxidation state. The Fe−O bond distances in **I** are in the range 2.144(2)−2.180(2) Å [$(Fe(1)-O)_{av.}$ = 2.144(2) Å and $(Fe(2)-O)_{av.}$ = 2.180(2) Å]. The Fe−F bond distances are in the range 2.0306(8)−2.0585(13), [$(Fe(1)-F)_{av.}$ = 2.0585(13) Å, and $(Fe(2)-F)_{av.}$ = 2.0429(5) Å]. The bond angle values show that all the iron atoms form near-perfect octahedra. Bond valence sum (BVS)[12] calculations [Fe(1) = 1.986 and Fe(2) = 1.981] as well as the values of the average bond distances indicate the oxidation states of Fe(1) and Fe(2) to be +2. The bond lengths and angles are in good agreement with those reported for the Fe^{2+}-

(7) (a) Selbin, J.; Holmes, L. H.; McGlynn, S. P. *J. Inorg. Nucl. Chem*. **1963**, *25*, 1359. (b) Nakamoto, K. *Infrared and Raman Spectra of Inorganic and Coordination Compounds*; Wiley: New York, 1978.

(8) Sheldrick, G. M. *SADABS: Siemens Area Detector Absorption Correction Program*; University of Göttingen: Göttingen, Germany, 1994.

(9) (a) Sheldrick, G. M. *SHELXS-86: Program for crystal structure determination*; University of Göttingen: Göttingen, Germany, 1986. (b) Sheldrick, G. M. *Acta Crystallogr., Sect A*. **1990**, *35*, 467.

(10) Sheldrick, G. M. *SHELXTL-PLUS Program for Crystal Structure Solution and Refinement*; University of Göttingen: Göttingen, Germany.

(11) (a) Dutrizac, J. E.; Kaiman, S. *Can. Mineral.* **1976**, *14*, 151. (b) Hawthrone, F. C.; Krivovichev, S. V.; Burns, P. C. *Rev. Mineral. Geochem*. **2000**, *40*, 1.

(12) (a) Brese, N. E.; O'Keeffe, M. *Acta Crystallogr*. **1991**, *B47*, 192. (b) Brown, I. D.; Altermatt, D. *Acta Crystallogr*. **1985**, *B41*, 244.

Table 2. Selected Bond Distances and Angles in $[H_3N(CH_2)_6NH_3][Fe^{II}_{1.5}F_3(SO_4)]\cdot 0.5H_2O$, I[a]

moiety	distance (Å)	moiety	distance (Å)
Fe(1)−F(2)$^{\#1}$	2.057(2)	Fe(2)−F(2)	2.056(2)
Fe(1)−F(2)$^{\#2}$	2.057(2)	Fe(2)−F(2)$^{\#4}$	2.056(2)
Fe(1)−F(2)	2.057(2)	Fe(2)−O(1)$^{\#4}$	2.180(2)
Fe(1)−F(2)$^{\#3}$	2.057(2)	Fe(2)−O(1)	2.180(2)
Fe(1)−O(2)	2.145(3)	S(1)−O(3)	1.444(3)
Fe(1)−O(2)$^{\#1}$	2.145(3)	S(1)−O(2)$^{\#1}$	1.487(3)
Fe(2)−F(1)$^{\#4}$	2.031(2)	S(1)−O(1)	1.489(2)
Fe(2)−F(1)	2.031(2)	S(1)−O(1)$^{\#3}$	1.489(2)
	Organic Moiety		
N(1)−C(1)	1.493(6)	C(4)−C(5)	1.529(6)
C(1)−C(2)	1.512(7)	C(5)−C(6)	1.507(6)
C(2)−C(3)	1.532(6)	C(6)−N(2)	1.501(5)
C(3)−C(4)	1.534(7)		

moiety	angle (deg)	moiety	angle (deg)
F(2)$^{\#1}$−Fe(1)−F(2)$^{\#2}$	91.94(9)	F(2)−Fe(2)-F(2)$^{\#4}$	180
F(2)$^{\#1}$−Fe(1)−F(2)	180	F(1)$^{\#4}$−Fe(2)−O(1)$^{\#4}$	94.43(8)
F(2)$^{\#2}$−Fe(1)−F(2)	88.06(9)	F(1)−Fe(2)-O(1)$^{\#4}$	85.57(8)
F(2)$^{\#1}$−Fe(1)−F(2)$^{\#3}$	88.06(9)	F(2)−Fe(2)-O(1)$^{\#4}$	86.68(7)
F(2)$^{\#2}$−Fe(1)−F(2)$^{\#3}$	180	F(2)$^{\#4}$−Fe(2)−O(1)$^{\#4}$	93.32(7)
F(2)−Fe(1)−F(2)$^{\#3}$	91.94(9)	F(1)$^{\#4}$−Fe(2)−O(1)	85.57(8)
F(2)$^{\#1}$−Fe(1)−O(2)	95.06(7)	F(1)−Fe(2)−O(1)	94.43(8)
F(2)$^{\#2}$−Fe(1)−O(2)	95.06(7)	F(2)−Fe(2)−O(1)	93.32(7)
F(2)−Fe(1)−O(2)	84.94(7)	F(2)$^{\#4}$−Fe(2)−O(1)	86.68(7)
F(2)$^{\#3}$−Fe(1)−O(2)	84.94(7)	O(1)$^{\#4}$−Fe(2)−O(1)	180
F(2)$^{\#1}$−Fe(1)−O(2)$^{\#1}$	84.94(7)	O(3)−S(1)−O(2)$^{\#1}$	110.0(2)
F(2)$^{\#2}$−Fe(1)−O(2)$^{\#1}$	84.94(7)	O(3)−S(1)−O(1)	110.27(7)
F(2)−Fe(1)−O(2)$^{\#1}$	95.06(7)	O(2)$^{\#1}$−S(1)−O(1)	108.71(8)
F(2)$^{\#3}$−Fe(1)−O(2)$^{\#1}$	95.06(7)	O(3)−S(1)−O(1)$^{\#3}$	110.27(8)
O(2)−Fe(1)−O(2)$^{\#1}$	180	O(2)$^{\#1}$−S(1)−O(1)$^{\#3}$	108.71(7)
F(1)$^{\#4}$−Fe(2)−F(1)	180	O(1)−S(1)−O(1)$^{\#3}$	108.9(2)
F(1)$^{\#4}$−Fe(2)−F(2)	87.13(8)	Fe(2)$^{\#5}$−F(1)−Fe(2)	129.07(8)
F(1)−Fe(2)−F(2)	92.87(8)	Fe(2)−F(2)−Fe(1)	127.88(8)
F(1)$^{\#4}$−Fe(2)−F(2)$^{\#4}$	92.86(8)	S(1)−O(1)−Fe(2)	130.04(2)
F(1)−Fe(2)−F(2)$^{\#4}$	87.13(8)	S(1)$^{\#1}$−O(2)−Fe(1)	129.5(2)
	Organic Moiety		
N(1)−C(1)−C(2)	110.6(4)	C(5)−C(4)−C(3)	112.7(4)
C(1)−C(2)−C(3)	111.3(4)	C(6)−C(5)−C(4)	110.2(4)
C(2)−C(3)−C(4)	111.3(4)	N(2)−C(6)−C(5)	111.2(3)

[a] Symmetry transformations used to generate equivalent atoms: (#1) $-x, -y, -z$; (#2) $-x, y, -z$; (#3) $x, -y, z$; (#4) $-x + {}^1/_2, -y + {}^1/_2, -z$; (#5) $-x + {}^1/_2, y - {}^1/_2, -z$.

Table 3. Hydrogen Bonding Interactions in Compound I

D−H...A	D−H	H...A	D...A	D−H...A
N(1)−H(1)...O(2)	0.90(3)	2.17(3)	3.043(5)	164(4)
N(1)−H(2)...O(1)	0.90(5)	2.13(5)	3.012(3)	165(7)
N(2)−H(9)...F(1)	0.89(2)	1.82(2)	2.715(5)	176(4)
N(2)−H(10)...F(2)	0.90(4)	1.89(5)	2.766(3)	164(6)

in fluorine and oxygen environments.[4d] The positions of the bridging F atoms are also supported by the bond valence calculations, which lie in the range 0.6−0.75. Thus, the framework stoichiometry of $[Fe^{II}_{1.5}F_3(SO_4)]$ with a −2 charge requires the amine to be doubly protonated.

The layers in **I** are stacked one over the other along the *c*-axis in *AAAA* fashion and held together by the N−H···O and N−H···F hydrogen bond (Figure 2) between the terminal ammonium groups and the framework oxygen and fluorine atoms. Other than the amines, extraframework water molecules also reside between the Kagomé slabs, which do not seem to form strong hydrogen bonds with the framework. Details of the probable hydrogen-bonding interactions are given in Table 3.

The presence of Fe in the +2 state in **I** is corroborated by the Mössbauer spectra. The spectra of **I** recorded at

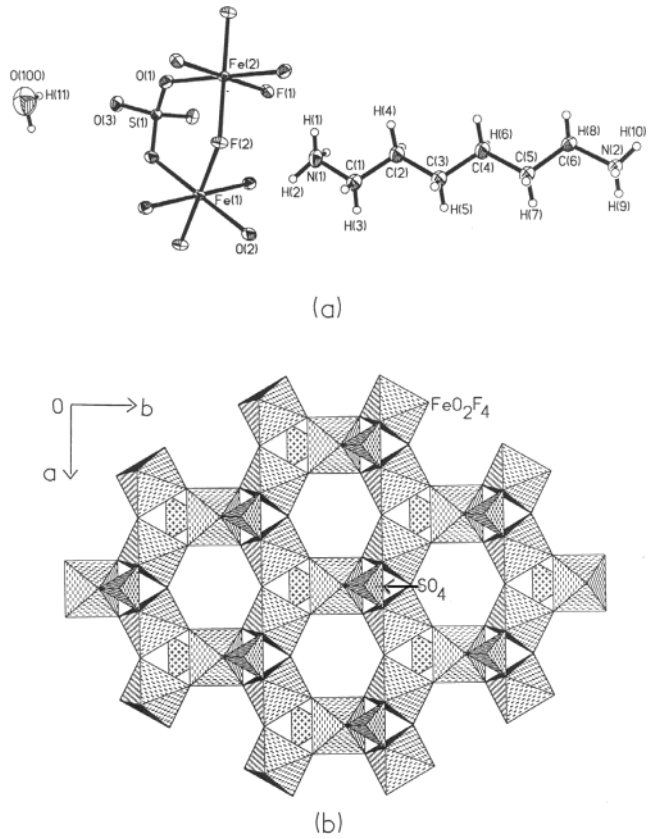

Figure 1. (a) ORTEP plot of $[H_3N(CH_2)_6NH_3][Fe^{II}_{1.5}F_3(SO_4)]\cdot 0.5H_2O$, **I**. The asymmetric unit is labeled. (b) Polyhedral view of **I** down the *c*-axis showing the Kagomé lattice. The three-membered apertures are capped by sulfate moieties.

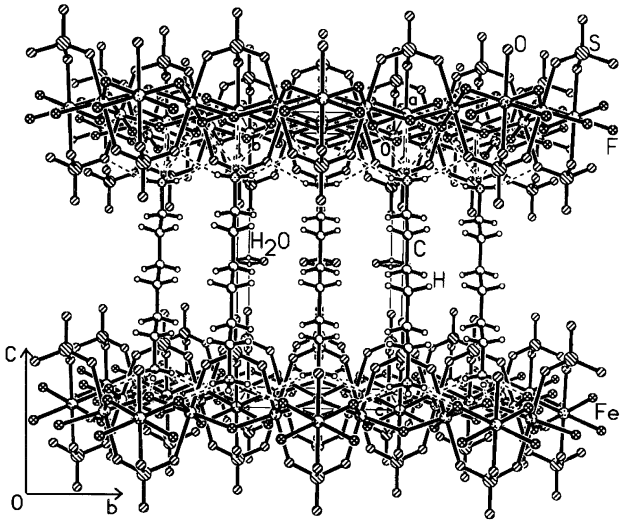

Figure 2. View along the *a*-axis showing the stacking of the layers pillared by the amine. Dotted line indicates H-bond interactions.

different temperatures are given in Figure 3. The spectra in the 20−300 K range show the presence of a single quadrupole-split spectrum. According to the crystallographic data, there should be two components with the theoretically expected proportion of 1:2. We therefore fitted the spectra for EFG for two sites with the intensity ratio constrained to 1:2, but with the same line width for the components. The refined parameters of the fitted spectra (isomer shift and quadrupolar splitting) at different temperatures are listed in Table

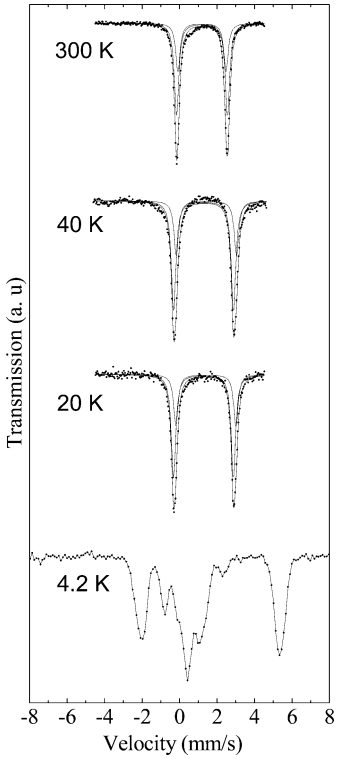

Figure 3. Mössbauer spectra of **I** recorded at 300, 40, 20, and 4.2 K.

Table 4. Mössbauer Parameters of I at Different Temperatures

temp (K)	isomer shift (IS1) (mm/s)	isomer shift (IS2) (mm/s)	quadrupole splitting (QS1) (mm/s)	quadrupole splitting (QS2) (mm/s)
298	+1.18	+1.19	2.57	2.74
40	+1.42	+1.26	3.21	3.19
20	+1.39	+1.26	3.20	3.19

4. The values of the isomer shift are consistent with those reported for high-spin Fe^{2+} ions in octahedral coordination, which is typically around 0.9−1.5 mm/s.[13,14] The quadrupole splitting increases with lowering temperature as in many of the Fe(II) compounds.[13] At this point it is necessary to compare the Mössbauer data of **I** with those of Fe^{3+} jarosites with the Kagomé lattice. The Mössbauer spectra of jarosites between 65 and 300 K, as reported in the literature, show two peaks with equal intensities with the isomer shift (IS) of 0.43−0.49 mm/s relative to pure Fe metal. The quadrupole splitting (QS) is in the range 1.15−1.24 mm/s.[15] The higher values of IS and QS in the case of **I** (Table 4) as typical for high spin Fe^{2+} in octahedral coordination establish the oxidation state of Fe in **I** to be +2. The spectrum of **I** shows evidence of magnetic ordering around 10 K. Thus, the spectrum at 4.2 K in Figure 3 clearly shows the emergence of hyperfine splitting. From the separation of the outermost lines, we have estimated the hyperfine field at 4.2 K to be 230 kOe. The spectrum is complex due to the mixing of quadrupolar and magnetic hyperfine splitting of comparable strengths. The magnetic hyperfine field at 4.2 K is not fully developed and a crossover of the hyperfine sublevels could make the central line more pronounced. This aspect along with the possibility of two hyperfine field components renders it difficult to analyze the spectrum reliably. This is in contrast to the Fe^{3+} jarosites, which give a symmetric six-line spectrum at 4.2 K.[15]

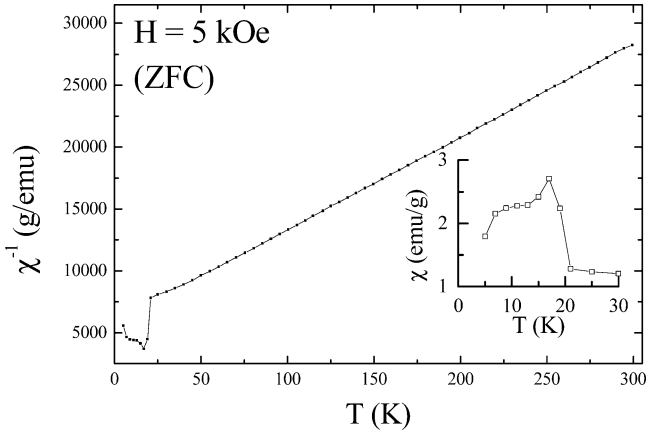

Figure 4. Inverse dc magnetic susceptibility (χ) of **I** (ZFC), measured in a field of 5 kOe. The inset shows the low-temperature $\chi(T)$ data in an expanded form.

The iron−sulfate system in the mineral kingdom is known to have rich structural chemistry.[11b] While the structures of the iron sulfates in nature comprise different dimensionalities, the 2-D Kagomé lattice of mineral jarosite, iron(III) sulfate has attracted special attention due to its interesting magnetic properties.[6] All the natural iron sulfates have a neutral or anionic framework of one, two, or three dimensions and the charge is balanced by the alkali cations or the ammonium ion. We have recently expanded the family of iron sulfates with extended structures by introducing the organo-ammonium cations which balance the negative charge of the framework and also act as a template. In this respect the discovery of a mixed valent (Fe^{2+} and Fe^{3+}) Kagomé lattice showing interesting magnetic behavior is noteworthy.[5]

The topology of **I** is identical to the Kagomé lattice of jarosite with Fe in the +3 oxidation state whereas Fe in **I** is in the +2 state. The organic template, $[H_2N-(CH_2)_6-NH_2]$, which is a long-chain diamine, keeps the Kagomé layers more than 13 Å away from one another. The Fe^{2+} sulfate, with a perfect Kagomé lattice, exhibits completely unique magnetic behavior compared to the Fe^{3+} Kagomé lattices as discussed below.

Magnetic Properties. The temperature dependence of the dc magnetic susceptibility (χ) data of **I** in the zero-field-cooled (ZFC) condition of the sample (measured at a magnetic field (H) of 5 kOe) are shown in Figure 4. The inverse χ varies linearly over the entire temperature range above 20 K, giving a paramagnetic Curie temperature (θ_p) of −75 K, suggesting dominant antiferromagnetic exchange interaction. The value of the effective magnetic moment (μ_{eff}) per Fe ion obtained from the Curie−Weiss region is 5.06 μ_B, which is close to the spin-only value of high-spin Fe^{2+} (4.89 μ_B) and is comparable to the values reported for similar compounds in the literature.[4d,16] This is to be compared with the magnetic moment of iron(III) jarosites which lies

(13) Greenwood, N. N.; Gibb, T. C. *Mössbauer spectroscopy*; Chapman and Hall: London, 1971.
(14) Riou-Cavellec, M.; Lesaint, C.; Nogues, M.; Grenèche, J.-M.; Férey, G. *Inorg. Chem.* **2003**, *42*, 5669.
(15) (a) Takano, M.; Shinjo, T.; Kiyama, M.; Takada, T. *J. Phys. Soc. Jpn.* **1968**, *25*, 902. (b) Takano, M.; Shinjo, T.; Takada, T. *J. Phys. Soc. Jpn.* **1971**, *30*, 1049. (c) Townsend, M. G.; Longworth, G.; Roudaut, E. *Phys. Rev. B* **1986**, *33*, 4919.

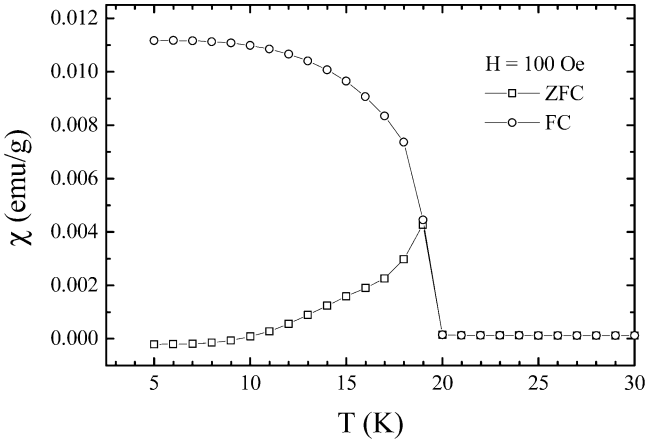

Figure 5. dc magnetic susceptibility measured in a field of 100 Oe for the zero-field-cooled (ZFC) and field-cooled (FC) conditions of **I**.

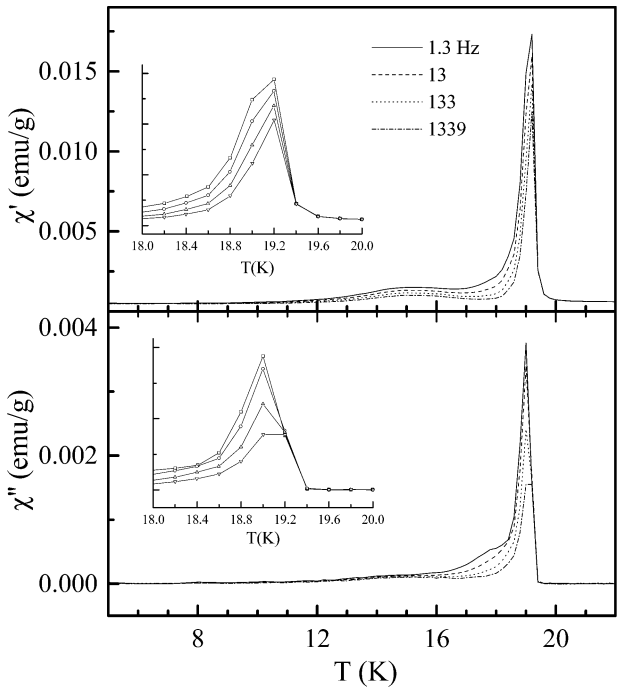

Figure 6. Real (χ') and imaginary (χ'') parts of ac susceptibility of **I** measured at different frequencies (ac field 5 Oe). The data around 19 K are shown in the inset in an expanded form.

in the range of 5.8−6.2 μ_B.[15b,17] There is a distinct deviation from the Curie−Weiss behavior below 20 K (see inset of Figure 4), as though there is an onset of magnetic ordering around 19 K. This ordering temperature is far below (one-fourth of) the value of θ_p, which implies that there is a competition from ferromagnetic coupling as well. This naturally leads to a question whether **I** undergoes spin-glass freezing. Interestingly, there is a shoulder in the $\chi(T)$ plot below 15 K, as though there is another magnetic transition. To understand the nature of these magnetic transitions, we have examined the irreversibility in the low-field ZFC−FC dc susceptibility, the isothermal magnetization (M), ac susceptibility, and isothermal remanent magnetization (M_{IRM}).

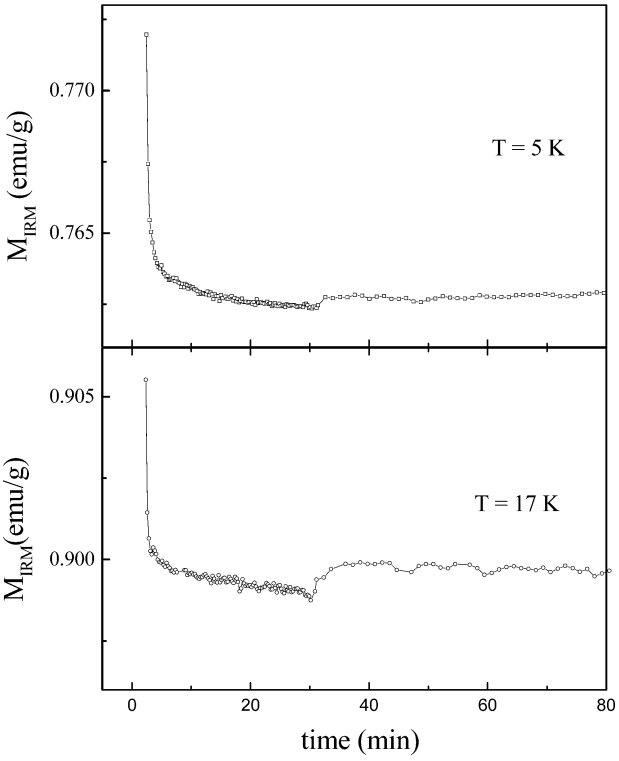

Figure 7. Isothermal remanent magnetization at 5 and 17 K for **I**, obtained as described in the text.

In Figure 5, the dc susceptibility of **I** measured in the presence of 100 Oe at both the ZFC and FC conditions is plotted. While there is a distinct feature due to the onset of a magnetic transition around 19 K, the shape of the $\chi(T)$ plot below 19 K in the FC condition is close to that expected of a ferromagnet. However, there is no corresponding ferromagnetic-like feature in the ZFC curve; instead, there is a bifurcation from the FC−$\chi(T)$ just below 19 K showing the existence of a irreversibility behavior, with a peak just below this temperature. The 15 K peak observed in the high field data (Figure 4) is not clearly visible, being masked by the broad curvature due to the 19 K transition. To explore whether the observed irreversibility behavior arises from spin-glass freezing or from domain-wall pinning effects often reported in long-range magnetically ordered systems, we have measured ac susceptibility as a function of frequency in the vicinity of the magnetic transitions (Figure 6). While the plots of both the real (χ') and the imaginary (χ'') parts exhibit narrow peaks at the onset of the magnetic transition around 19 K, there is a distinct peak, though broad, around 15 K, as in the case of the high-field dc χ data (see Figure 4). The most notable feature in the ac χ data is that there is no noticeable frequency dependence of the peak temperatures for both the transitions, as revealed by the plots shown in an expanded form in the inset of Figure 6, for the 19 K transition. This observation demonstrates that **I** does not undergo spin-glass freezing in the temperature range of investigation.

We have also measured the isothermal remanent magnetization, M_{IRM}, at two temperatures, 5 and 17 K. For this purpose, we cooled the specimen from 50 K to the desired temperature in zero magnetic field, switched on the field of 5 kOe for 5 min, and then measured the remanent magnetization for about 80 min after switch-

(16) Fu, A.; Huang, X.; Li, J.; Yuen, T.; Lin, C. L.*Chem. Eur. J.* **2002**, *8*, 2239.
(17) Grohol, D.; Nocera, D. G.; Papoutsakis, D. *Phys. Rev. B* **2003**, *67*, 64401.

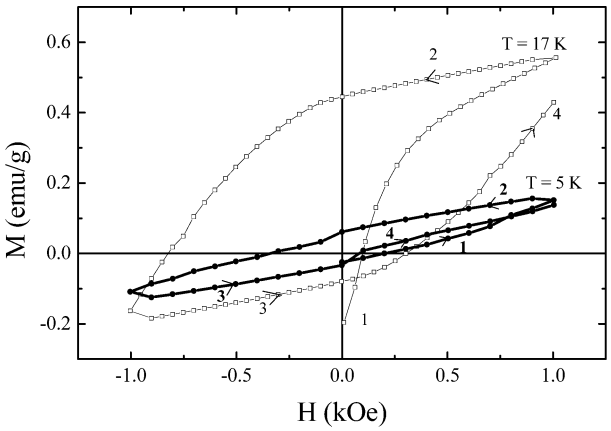

Figure 8. Hysteresis loops (ZFC) for of **I** at 5 and 17 K. The arrows (marked 1, 2, 3, and 4) are shown to follow the way the magnetic field was varied. The data at 5 K are shown by the bold curve (with bold numbers).

ing off the field. The M_{IRM} behavior thus obtained as a function of time (t) is shown in Figure 7. It may be mentioned that it takes about 1 or 2 min for the magnetometer to reduce the field to zero and the $t = 0$ point in Figure 7 corresponds to a time after this small time lag. The point to note is that, after the magnet is switched off, M_{IRM} sharply drops within a few minutes at both the temperatures, remaining constant thereafter. If **I** was a spin-glass, M_{IRM} would have exhibited a slow decay.[18,19] This finding establishes that the 15 and 19 K features in **I** are not due to spin-glass-like freezing.

A careful look at the isothermal dc (ZFC) magnetization data of **I** is also revealing. There is a distinct hysteresis in the low-field (<1 kOe) data recorded at 5 and 17 K (Figure 8). This suggests the presence of a ferromagnetic component, though the size of the hysteresis loop is considerably smaller at 5 K. We, however, find M varies rather linearly until the highest field measured without any evidence for saturation, thereby establishing that there is a significant antiferromagnetic component as well, in conformity with the negative θ_p. In addition, the value of magnetic moment per Fe even in a field of 60 kOe in the apparent magnetically ordered state is less than 0.3 μ_B. All these findings, including the isothermal M behavior, can be reconciled if the ordering below 19 K is ferrimagnetic, with a possible small change in the magnetic structure below 15 K.

Conclusions

An iron(II) sulfate with the perfect Kagomé lattice has been synthesized. Magnetic properties of this material are distinctly different from those of the Fe(III) sulfates possessing the Kagomé lattice. Unlike the Fe(III) Kagomé compounds, which show magnetic frustration or antiferromagnetism at low temperatures, the Fe(II) Kagomé compound synthesized by us becomes ferrimagnetic around 19 K, undergoing a change in magnetic structure below 15 K. It does not exhibit spin-glass freezing. It would be worthwhile to carry out a neutron diffraction study of the compound to delineate the magnetic structure.

Acknowledgment. The authors thank DRDO (India) for support of this research.

Supporting Information Available: X-ray crystallographic file in CIF format for the structure determination of **I**. This material is available free of charge via the Internet at http://pubs.acs.org.

CM035304+

(18) Mydosh, J. A. *Spin Glasses: An Experimental Introduction*; Taylor and Francis: London, 1993.
(19) Binder, K.; Young, A. P. *Rev. Mod. Phys.* **1986**, *58*, 801.